Order–Disorder Transitions Confined at the Interface of Pd@Co Core–Shell Nanoparticles: Implications for Magnetic Recording

Kazuhisa Sato*[,†,‡] and Hidehiro Yasuda[†,‡]

[†]Research Center for Ultra-High Voltage Electron Microscopy, Osaka University, 7-1 Mihogaoka, Ibaraki, Osaka 567-0047, Japan

[‡]Division of Materials and Manufacturing Science, Graduate School of Engineering, Osaka University, 2-1 Yamadaoka, Suita, Osaka 565-0871, Japan

*Corresponding Author: sato@uhvem.osaka-u.ac.jp

ABSTRACT:

We observed an order–disorder transition confined to the interface of Pd@Co core–shell nanoparticles with a Pd core and Co shell. A local ordered region with the $L1_0$- and $L1_2$-type ordered structure 2–3 nm in size was formed in a ~12-nm-sized particle. The local atomic order was only achieved in the narrow temperature range of 573–723 K, where the diffusion length is limited to a short range comparable to the nearest-neighbor distance of the Co–Pd solid solution. Once the atom migration was activated ($T \geq 773$ K), alloying of Co and Pd proceeded rapidly, and the ordered phase disappeared along with the core–shell structure. Namely, the stability of the ordered phase was diffusion controlled. Chemically sensitive atomic-resolution electron microscopy enabled detection of the local atomic order formed in a nanoparticle. Such local atomic order has the potential to enable tuning of the magnetic anisotropy of bimetallic nanomagnets, which may open a new route to realize ultrahigh density magnetic storage media.

KEYWORDS: *short-range order, core–shell structure, nanoparticle, order–disorder transition, HAADF-STEM*

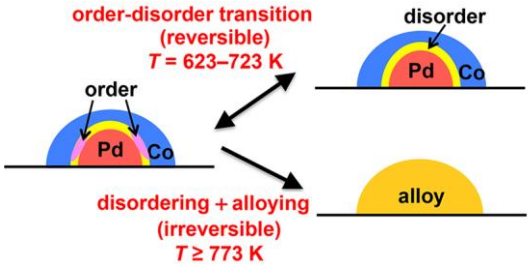

INTRODUCTION

Bimetallic nanoparticles composed of a ferromagnetic 3d transition metal (Fe, Co, Ni) and a noble metal (Au, Pt, Pd, Ru) have been extensively investigated in terms of their novel magnetic and catalytic properties as well as their structures[1]. Among these binary systems, alloy nanoparticles with the tetragonal $L1_0$-type (AuCu I-type) ordered structure, such as Fe–Pt, Co–Pt, and Fe–Pd, have received particular attention as ultra-high-density magnetic storage materials. Abundant knowledge has been accumulated on their atomic structures, phase transitions, and magnetic properties in the last two decades[1-3].

However, limited studies have been performed on Co–Pd nanoparticles compared with those on Fe–Pt or Co–Pt systems, with most focusing on catalytic applications using the core–shell structure[4-7]. This absence of research is presumably because the Co–Pd alloy forms a solid solution in thermal equilibrium unlike the aforementioned FePt and similar compounds and does not exhibit outstanding magnetic properties, which are of interest from a technical viewpoint[8]. According to the binary alloy phase diagram[9], Co–Pd alloy forms a solid solution phase over the entire composition range, so there is no ordered phase or intermetallic compound between Co and Pd that can be a source of excellent magnetic properties. This situation is similar to the case of Ni-Pd system, which also forms solid solution in all the composition range[10]. In fact, Ni-Pd nanoparticles are famous as catalysts[11-13], but their potential as magnetic materials is unknown. However, near a half a century ago, short-range order (SRO) was identified in Co–Pd bulk alloys according to analysis using diffuse scattering of X-rays[14]. In addition, a previous electron diffraction study revealed the existence of long-range order (LRO), namely, both $L1_0$- and $L1_2$-type ($AuCu_3$-type) ordered structures, in vacuum-deposited Co–Pd thin films[15]. Such atomic ordering may increase the magnetic anisotropy of Co–Pd alloy thin films or nanoparticles, as the magnetocrystalline anisotropy energy (K_U) is proportional to the square of the

degree of order (S), namely $K_U \propto S^2$ [16]. Local atomic ordering has the potential to open a new route for the synthesis of nanomagnets with potential application in ultrahigh-density magnetic storage media. However, after these pioneering works, no further studies were published on this topic, and hence, the possible existence of atomic ordering in Co–Pd alloy remains an open question.

Figures 1a and 1b show the crystal structures of the $L1_2$- and $L1_0$-type ordered structures, respectively. High-resolution electron microscopy (HREM) combined with computational models is considered an indispensable technique to characterize the local ordered structures in alloys[17, 18]. In addition to the established methods, high-angle annular dark-field scanning transmission electron microscopy (HAADF-STEM) enables the direct identification of atomic species in a multicomponent alloy[19] as well as in bimetallic nanoparticles[20-22]. As shown in the simulated images for the $L1_2$-type $CoPd_3$ (Figure 1c) and $L1_0$-type CoPd (Figures 1d and 1e) ordered phases, the constituent elements and their arrangements can be directly identified by the atomic number (Z) contrast: heavier Pd (Z = 46) appears with brighter contrast than Co (Z = 27).

Nanoparticles with a core–shell structure can be regarded as a diffusion couple at the nanoscale, and hence, the particle interfacial area between the core and shell will include various local atomic structures. The purpose of this study was to elucidate the local atomic structures of Pd@Co core–shell nanoparticles with a Pd core and Co shell in an attempt to unlock the potential of Co-Pd nanoparticles as nanomagnets. We show that both $L1_0$- and $L1_2$-type ordered structures are locally formed in Pd@Co nanoparticles and discuss the thermal stability of the local ordered structures.

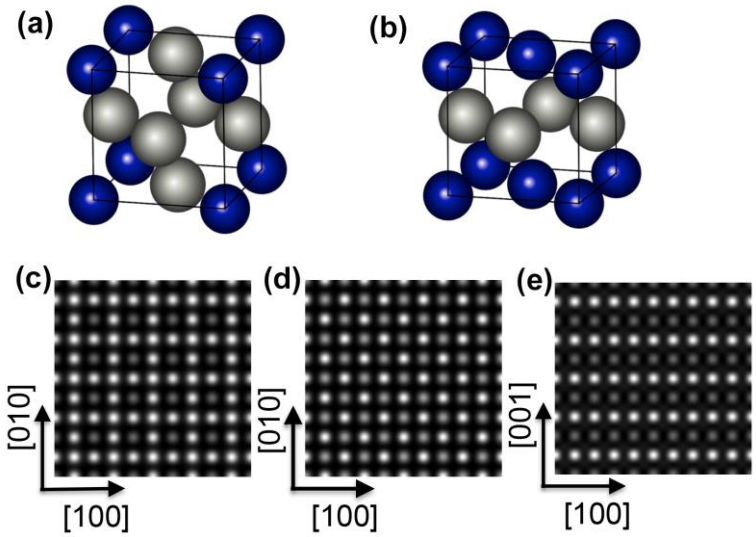

Figure 1. $L1_2$-type (a) and $L1_0$-type (b) ordered structures. Simulated HAADF-STEM images of $L1_2$-$CoPd_3$ (c) and $L1_0$-CoPd (d, e): (c) $L1_2$, beam incidence in the [001] direction, (d) $L1_0$, [001], and (e) $L1_0$, [010]. Periodic arrangements of Pd and Co atoms are observed.

RESULTS

Figure 2a presents a selected area electron diffraction (SAED) pattern of the as-deposited Pd@Co nanoparticles with Pd content of 44 at% covered by a thin amorphous (a-) Al_2O_3 film. Deposition was performed at 573 K. The SAED pattern consists of reflections of Pd and Co together with weak halo rings from the a-Al_2O_3 film. Note that both Pd and Co adopt the face-centered cubic (fcc) structure. The following cube-on-cube orientation relationships are observed between fcc-Co and fcc-Pd: $<100>_{Co}$ // $<100>_{Pd}$, $\{001\}_{Co}$ // $\{001\}_{Pd}$. This is due to the epitaxial growth of Pd on the NaCl(001) substrate maintained at 573 K, followed by growth of Co in the sequential deposition process of Pd, Co, and Al_2O_3. A magnified image of the pattern near the 220_{Pd} and the 220_{Co} reflections is presented in the lower inset. The coexistence of 220_{Pd} and 220_{Co} is clearly observed. Note that the 200 reflections of Co and Pd are close in distance and hence overlap with each other. The difference in

the reflection intensity between Co and Pd is mainly due to the difference in magnitude of the atomic scattering factors (f) between Co and Pd ($f_{Pd} > f_{Co}$). The weak reflections indicated by the arrowheads correspond to {111} stacking faults, which is frequently formed in metals and alloys with the fcc structure[21]. Figure 2b presents a HAADF-STEM image of the Pd@Co nanoparticles (same sample as that for the SAED pattern in Figure 2a). The average particle size was 6.8 ± 1.3 nm in diameter with a particle areal density (surface density) of 2.1×10^{11} cm^{-2}. Most of the particles showed core–shell contrast. Figure 2c presents an atomic-resolution HAADF-STEM image of a representative Pd@Co nanoparticle with core–shell contrast. The Z-contrast directly reveals the formation of a Pd core (bright contrast) and Co shell (weak contrast). Atomic columns of Co and Pd were connected smoothly because of the epitaxial growth of Co and Pd. Electron energy-loss spectroscopy (EELS) revealed that core-loss spectra of Co ($L_{2,3}$ edge) were detected from the entire particle including the particle center. Figure 2d presents a typical core-loss spectrum of the Co-$L_{2,3}$ edge obtained from the central area of the particle shown in the inset. Based on the HAADF-STEM imaging and EELS analysis, we deduced the particle shape depicted in the schematic illustration in the inset of Figure 2b, where the Co shell covers the Pd core in a hemispherical form.

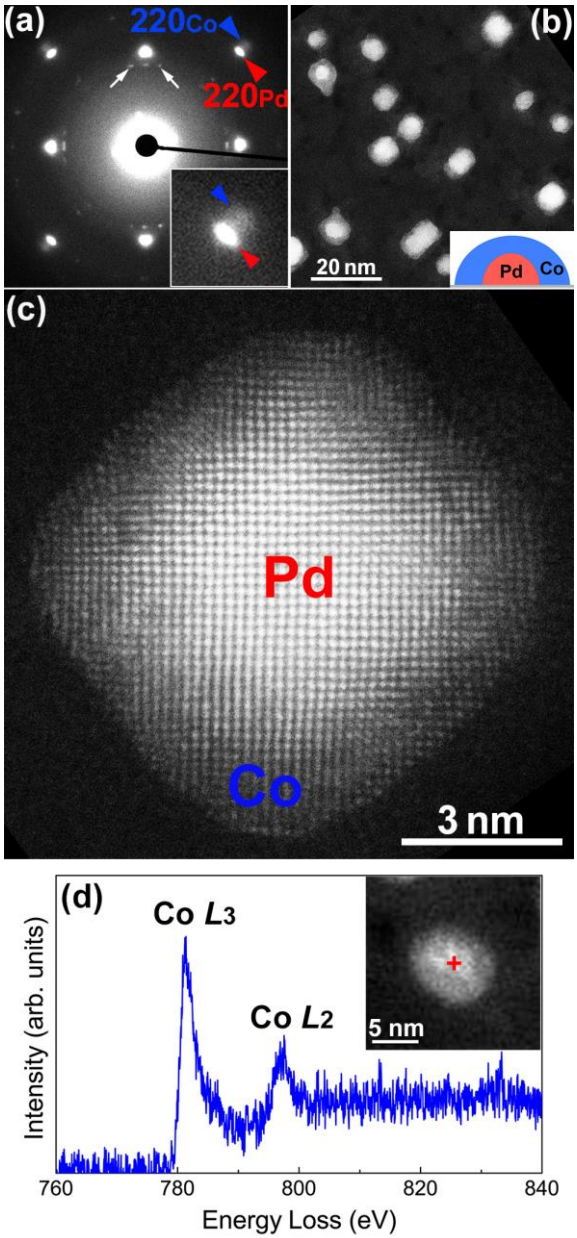

Figure 2. (a) SAED pattern of the as-deposited Pd@Co nanoparticles with an average Pd content of 44 at%. (b) HAADF-STEM image of Pd@Co nanoparticles. The inset presents a schematic illustration of the cross-section of the hemispherical core–shell structure. (c) Atomic-resolution HAADF-STEM image of a representative Pd@Co nanoparticle with core–shell contrast. (d) Core-loss spectrum of Co-$L_{2,3}$ edge obtained from the central area of the particle shown in the inset. The observations were performed at room temperature.

Annealing of the as-deposited Pd@Co nanoparticles led to the formation of alloy nanoparticles. The intensity of the 220_{Co} reflection became weak and disappeared at 773 K, indicating dissolution of Co into Pd. In fact, the lattice parameter of the alloy phase formed by annealing at 823 K for 300 s was almost the same as that of the as-deposited Pd (a = 0.39 nm). The average particle size was 7.1 ± 1.6 nm in diameter with a particle areal density of 2.2×10^{11} cm^{-2}. The insignificant particle coalescence and growth indicate that the alloying reaction proceeded within each nanoparticle. Figure 3a presents an SAED pattern of the nanoparticles after annealing at 823 K for 300 s (same sample as that shown in Fig. 2). A magnified image of the pattern near the 220 reflection is presented in the lower inset. The splitting of the 220_{Co} and 220_{Pd} reflections observed in the as-deposited specimen (Figure 2a) disappeared, indicating alloying of Co and Pd. The weak streaks indicated by arrowheads originate from {111} stacking faults. The atomic-resolution HAADF-STEM image in Figure 3b shows that the core–shell contrast disappeared with alloy phase formation. The image contrast was lower at the peripheral region of the particle because of the particle shape and differed from the core–shell contrast. Figure 3c presents a magnified HAADF-STEM image. There are two types of contrast in the atomic columns, as indicated by the red and blue arrowheads. The red arrowhead indicates an atomic column with strong bright contrast, and similar contrast spots are randomly distributed. These bright spots can be attributed to Pd atoms in a solid solution of Co–Pd alloy, whereas there is no local atomic order in the annealed specimen. It is also noted that no superlattice reflection of the ordered phase was detected during the *in-situ* annealing.

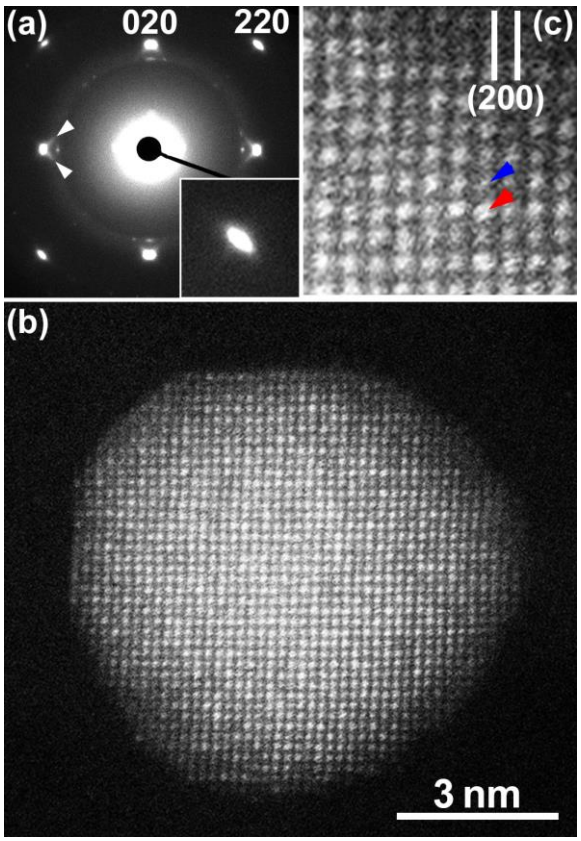

Figure 3. (a) SAED pattern of the nanoparticles after annealing at 823 K for 300 s. A magnified image of the pattern around the 220 reflection is shown in the lower inset. An alloy phase was formed. (b) Atomic-resolution HAADF-STEM image of a representative Co–Pd alloy nanoparticle. (c) Magnified HAADF-STEM image. There were two types of contrast in the atomic columns, as indicated by the red and blue arrowheads. The observations were performed at room temperature.

Figure 4a presents an SAED pattern of the as-deposited Pd@Co nanoparticles with a Pd content of 88 at%. Deposition was performed at 623 K. The average particle size was 11.9 ± 2.0 nm in diameter with a particle areal density of 1.3×10^{11} cm^{-2}. The existence of pure Co is not certain because the 220_{Co} reflection cannot be identified. This is most likely due to the low Co concentration (12at%) and possible alloying of Co and Pd during the particle growth at 623 K. A noticeable feature

is the existence of weak satellite reflections in addition to strong fundamental reflections. These satellite reflections can be indexed as 100 and 110 superlattice reflections of the $L1_2$-type ordered structure. Namely, the ordered phase was formed by particle growth at 623 K during the sequential deposition of Pd and Co. The weak streaks due to {111} stacking faults are indicated by arrows. Figure 4b presents an atomic-resolution HAADF-STEM image of a representative Pd@Co nanoparticle. The core–shell contrast is still apparent; however, the $L1_2$-type ordered phase is formed at the peripheral region of the nanoparticle. The ordered region is narrow, approximately 2–3 nm in size. A magnified image of the ordered region is shown in the lower-left inset. The arrangement of bright spots is consistent with the simulated image shown in Figure 1c. An anti-phase boundary (APB) was observed along the line between the blue and red arrowheads. A magnified image of the area including the APB is shown in the upper-right inset. The APB is indicated by the dotted line. The atomic rows indicated by the blue arrowheads shifted a half period of the lattice at the APB with respect to the rows indicated by the red arrowheads. It should be noted that existence of the APB provides evidence that the ordered phase was formed by the nucleation and growth mechanism[23]. The fast Fourier transform (FFT) pattern of this image in Figure 4c includes clear 100 and 110 superlattice reflections in addition to the fundamental reflections.

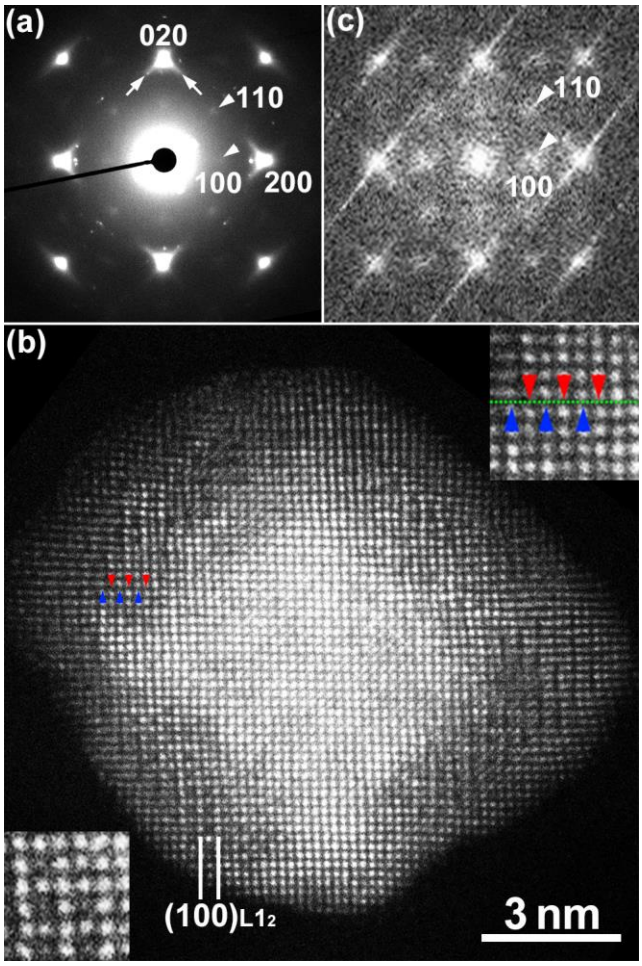

Figure 4. (a) SAED pattern of the as-deposited Pd@Co nanoparticles with an average Pd content of 88 at%. Superlattice reflections of the $L1_2$-type ordered structure are observed. (b) Atomic-resolution HAADF-STEM image of a representative Pd@Co nanoparticle including local ordered region. (c) FFT pattern of the image shown in (b). The observations were performed at room temperature.

Figure 5 provides another example of the Pd@Co nanoparticle including an ordered phase (same sample as that shown in Figure 4). The $L1_2$-type ordered phase is formed on the right side of the nanoparticle. A magnified image is shown in the upper-right corner. However, the $L1_0$-type ordered phase was observed at the upper-left part of the nanoparticle. A magnified image is presented in the lower left corner. The atomic arrangements of these ordered regions are consistent with the simulated

ones shown in Figures 1c ($L1_2$, [001] zone) and 1e ($L1_0$, [010] zone). The following lattice parameters were deduced: a = 0.39 nm for the $L1_2$-$CoPd_3$ and a = 0.39 nm, c = 0.38 nm, with c/a = 0.97 for the $L1_0$-CoPd. The accuracy of these measurements was 0.01 nm. The superlattice reflections of the $L1_2$-$CoPd_3$ and $L1_0$-CoPd structures overlapped with each other in the SAED pattern (Figure 4a). Thus, as shown in Figures 4 and 5, we observed that the ordered phase was formed in the Pd@Co core–shell nanoparticles and was confined to a region of less than a few nanometers. Such a small ordered region is rather similar to SRO and largely differs from the case of CoPt or FePd nanoparticles with well-developed LRO. Such local atomic ordering is in good agreement with the report by Katsnel'son et al. for bulk Co–75at%Pd alloy with ordered regions of 1.5–2 nm in size[14]. These researchers stated that the size of the ordered region is intermediate between normal LRO and SRO and termed the region "local order". The coexistence of the $L1_0$ and $L1_2$ phases is consistent with another study where two-phase coexistence was reported in Co–Pd alloy thin films with a Pd content of 60–70 at%[15].

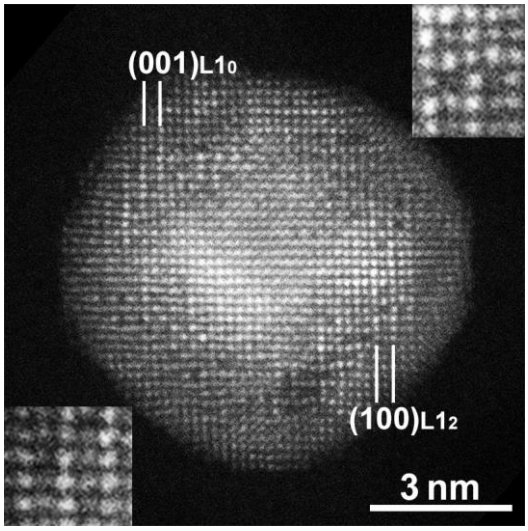

Figure 5. Atomic-resolution HAADF-STEM image of a representative Pd@Co nanoparticle including local ordered region. Magnified images of the $L1_2$ (upper right corner) and $L1_0$ ordered regions (lower left corner) are also shown. The observations were performed at room temperature.

Figure 6 shows the presence or absence of the ordered phase in as-deposited Pd@Co nanoparticles with respect to the Pd concentration and substrate temperature during the particle growth. The data points in Figure 6 were obtained for nanoparticles with average particle sizes of 9–16 nm in diameter. The ordered phase formation was judged by the existence of superlattice reflections in the SAED patterns (represented by open circles (○)). An open triangle (△) indicates that the local ordered region was detected by HAADF-STEM while the superlattice reflections were invisible in SAED. A cross mark (×) indicates that no ordered phase was detected by SAED or HAADF-STEM. The type of the ordered structure was determined by atomic-resolution HAADF-STEM analysis. As observed, particle growth above 623 K led to the formation of the ordered phase. Namely, interfacial atomic ordering is a thermally activated process. Both the $L1_2$ and $L1_0$ structures were identified when the ordered phase was detected (○ and △). Atomic ordering was detected for specimens with Pd contents higher than 59 at%. The ordered phase was also detected for a specimen deposited at 573 K when the Pd content was high (75 at%Pd). This result suggests that the interfacial atomic ordering may depend on the Pd content despite the sequential deposition where pure Co is always supplied onto the pure Pd seed. In contrast, the ordered phase was not observed for specimens with lower Pd contents (36–51 at%Pd). Furthermore, atomic ordering was not detected for post-deposition annealing up to 823 K (Co–44 at%Pd, Figure 3).

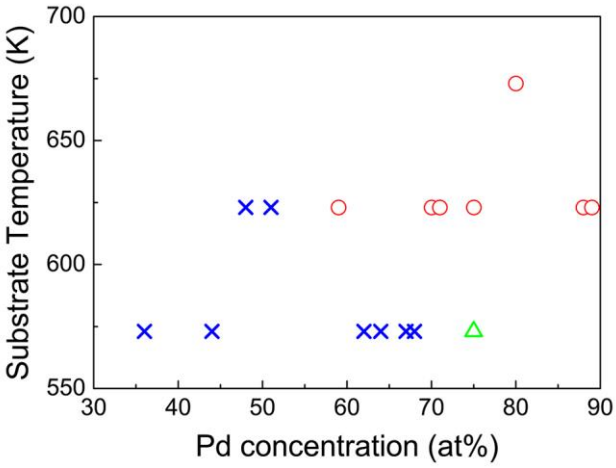

Figure 6. Presence or absence of ordered phase with respect to Pd concentration and substrate temperature during particle growth. Open circle (○): superlattice reflections were included in the SAED pattern, Open triangle (△): superlattice reflections were invisible in the SAED pattern, but a local ordered region was detected by HAADF-STEM, Cross mark (×): ordered structures were not detected by SAED nor HAADF-STEM.

Figure 7 shows the temperature dependence of the diffracted beam intensity profiles of the Co–88at%Pd nanoparticles near the 110 superlattice reflection (same sample as that shown in Fig. 4 and 5). The deposition temperature was 623 K. The profiles were measured in the [hh0]* direction in the SAED pattern obtained by *in-situ* annealing in the TEM. The intensity of the 110 reflection remained almost constant upon annealing up to 698 K, indicating that the local ordered region was hardly developed by annealing. Namely, the SRO in Co–Pd nanoparticles does not evolve into LRO by post-deposition annealing. The 110 reflection disappeared at 723 K, providing clear evidence that the ordered phase became disordered by annealing. After holding for 300 s at 723 K, the specimen was cooled down to room temperature. The 110 superlattice reflection appeared again at 623 K during the cooling process. The observed reversible change of the superlattice reflections indicates that the

structural change on annealing results from order–disorder transition. It is inferred that the transition occurs in a narrow interfacial area between the Pd core and Co shell in the Pd@Co nanoparticles. The transition temperature (T_c) is approximately 723 K, which is lower than that (T_c = 1103 K) reported for a Co–80at%Pd alloy thin film[15]. We confirmed the reproducibility of the disappearance and appearance of the superlattice reflections as a function of temperature. Such a sudden change in the intensity of superlattice reflections at T_c is a characteristic of a cooperative phenomenon. The temperature dependence of the SRO can be represented by statistical thermodynamic theory[24, 25]. We also noticed that once the specimen is heated to 773 K, the superlattice reflections never appear again during the cooling process. This phenomenon will be discussed later from the viewpoint of atom diffusion. The particle size and particle areal density were conserved during the annealing process.

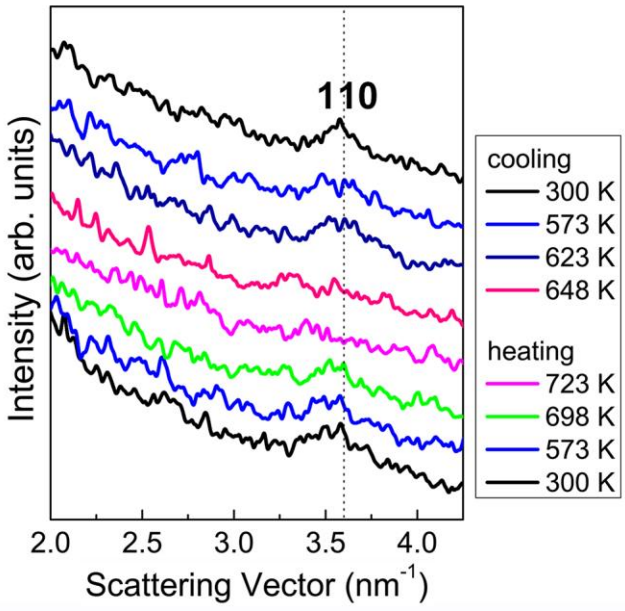

Figure 7. Temperature dependence of diffracted beam intensity profiles obtained by *in-situ* annealing in the TEM. The 110 superlattice reflection disappeared at 723 K during the heating process and it appeared again at 623 K during the cooling process. The deposition temperature was 623 K.

DISCUSSION

Nanoparticle Growth and Diffusion Length. For the particle morphology, it should be noted that in our sequential electron-beam (EB) deposition taking advantage of the epitaxial growth of metal nanoparticles on a NaCl(001) substrate, Pd nanoparticles act as nucleation sites for later deposited Co[26]. This is the origin of the formation of the Pd-core with Co-shell nanoparticles in this study. The particle growth condition largely differs from the cases reported in the literature: a Pd shell was formed when deposition was performed at room temperature[5, 6]. Significant differences of these studies from our study are that Co was deposited first, and the nanoparticles were grown at room temperature on NiAl[5] or Al_2O_3 substrates[6]. In general, it is presumed that a constituent element with the lower surface free energy (γ) prefers to form a shell to minimize the total Gibbs free energy of a particle/substrate system (for Pd@Co, γ_{Pd} = 2.05 J/m^2 < γ_{Co} = 3.23 J/m^2 [27]). However, core-shell structure is not thermally stable in the case of Co-Pd system since Co and Pd are miscible with each other in all the composition range[9]. Therefore, it is inferred that the Pd@Co core-shell structure is determined by kinetics rather than surface free energy. Interdiffusion of Co and Pd will be dominant compared to the Pd segregation towards the particle surface in the case of Pd@Co nanoparticles grown at 573–673 K. Surface segregation of a constituent element with a lower surface free energy has been observed in Au@Co nanoparticles prepared by the same technique (Au shell was formed irrespective of the deposition sequence when the particle size was smaller than 11 nm)[22]. In this case, Co and Au are immiscible with each other and phase separation occurs by annealing. In any case, the prerequisite for island growth is that the surface free energy of the substrate must be lower than that of the constituent elements. It is also noted that the interfacial free energy between the core and shell may play an essential role in determining the particle morphology.

The formation of the ordered phase clearly indicates that a compositional gradient exists at the

interface between the Pd core and Co shell, namely the interface is not steep with respect to chemical composition but rather an alloy phase exists between Pd and Co. If the enthalpy of mixing is negative, the SRO state can be realized[28]. The heat of formation for Co–Pd alloy is actually a small negative value (−2 kJ/mol)[29]. Such an alloy phase is formed during the particle growth above 623 K. Hence, atom diffusion is a key issue to clarify the observed atomic ordering. We estimated the diffusion length L for Co–Pd alloy using the following equations:

$$D = D_0 exp(-\frac{Q}{k_B T}) \quad (1)$$

$$L = \sqrt{Dt}, \quad (2)$$

where D denotes the diffusion coefficient for interdiffusion in Co–Pd alloy, D_0 is the frequency factor, Q is the activation energy, k_B is the Boltzmann constant, T is the temperature, and t is the time. The values of D_0 and Q for Co–Pd bulk alloy have been reported in the temperature range between 1153 K and 1466 K[30]. We estimated the diffusion length in the temperature range between 573 K and 773 K assuming Q = 238.1 kJ/mol and $D_0 = 4.24 \times 10^{-5}$ $m^2 s^{-1}$ for Co–75at%Pd alloy after the values reported in the literature (the aforementioned value is the arithmetical mean of the reported values for 70at%Pd and 80at%Pd alloys)[30]. The obtained results are listed in Table I. A diffusion time of 600 s at each temperature was assumed for the calculation based on the experiments in this study (EB deposition and *in-situ* annealing in the TEM).

Table 1. Temperature (T) and estimated diffusion length (L) for Co–75at%Pd and experimentally observed structural changes. A diffusion time of 600 s was assumed.

T / K	L / nm	Structural changes
573	2.2×10^{-3}	–Epitaxial growth of Pd and Co by EB deposition (Figure 2)
623	1.6×10^{-2}	–Epitaxial growth of Pd and Co by EB deposition –Formation of local atomic order during the particle growth (Figures 4 and 5) –Re-appearance of the superlattice reflections in the cooling process (Figure 7)
673	9.0×10^{-2}	–Epitaxial growth of Pd and Co by EB deposition –Formation of local atomic order during the particle growth (Figure 6)
723	3.9×10^{-1}	–Disappearance of the superlattice reflections in the heating process (Figure 7)
773	1.4	–Disappearance of core-shell structure
823	4.4	–Alloy phase formation (Figure 3)

As observed, it is practically difficult to promote atom migration at 573–673 K via a vacancy process, and hence, surface diffusion will dominate interfacial ordering as well as particle growth during the EB deposition. The absence of the superlattice reflections in the specimen deposited at 573 K indicates that a substrate temperature of 573 K is insufficient to promote interfacial mixing of atoms. The superlattice reflections disappeared at 723 K with post-deposition annealing. The estimated diffusion length at 723 K is 0.39 nm, which corresponds to the second-nearest-neighbor distance in the Co–Pd alloy. The estimated diffusion length reminds us of the fact that order–disorder transition in an alloy is the typical cooperative phenomenon and hence does not require long-range atom migration. At 773 K, structural change in nanoparticles by interdiffusion is possible as the estimated diffusion length exceeds 1 nm. This is consistent with the experimental result that the core–shell structure disappeared after annealing at 773 K for 600 s. Such an interfacial reaction reduces the

compositional gradient in a nanoparticle, and eventually, compositionally homogeneous nanoparticles are formed. Once the temperature was raised to 773 K, the superlattice reflections did not reappear during the cooling process. This finding can be explained by the remarkable deviation of the interfacial composition from the composition range necessary for the ordered phase formation. In the temperature range where the order–disorder transition occurs as a cooperative phenomenon (namely, ~723 K in this study), large-scale interfacial atom diffusion is practically impossible. This appears to allow the occurrence of the order–disorder transition in a core–shell nanoparticle. The aforementioned processes are summarized in Figure 8: (a) an as-deposited core–shell nanoparticle with local atomic order, (b) disordered phase formation by order–disorder transition (T = 623–723 K), (c) disordering together with alloying ($T \geq$ 773 K), (d) alloy phase (solid-solution) formation. Reversible transition is possible in the temperature range between 623 and 723 K.

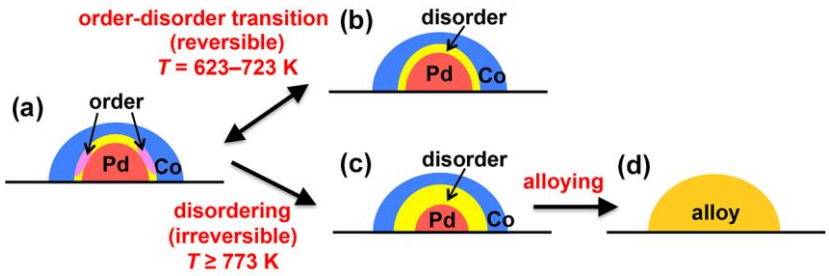

Figure 8. Schematic illustration of the structural changes of a Pd@Co core–shell nanoparticle: (a) as-deposited core–shell nanoparticle with local atomic order, (b) disordered phase formation by order–disorder transition (T = 623–723 K), (c) disordering together with alloying ($T \geq$ 773 K), (d) alloy phase (solid-solution) formation.

In the sequential deposition process employed in this study, a pure Co layer is formed on the pure

Pd seed irrespective of the amount of deposited Co. In this respect, alloy composition dependence of the ordered phase formation should not appear. However, we detected superlattice reflections of the ordered phase in the specimen with Pd concentration of 59–89 at%. To explain this result, we presume that the ordered phase is formed at the beginning of Co deposition; however, once the Co content exceeds a critical value, the alloy composition at the interfacial area deviates from the formation range of the $L1_0$- or $L1_2$-type ordered phase owing to the interdiffusion of Co and Pd at the interface. That is, when the Co concentration is 11–41 at%, the composition of the interfacial alloy layer matches the formation range of $L1_0$-CoPd or $L1_2$-$CoPd_3$. In contrast, in a Co-rich concentration, it is presumed that the concentration of the interfacial layer may deviate from the formation range of the ordered phase. The composition of the interfacial layer is determined by surface diffusion during particle growth. It should be noted that spontaneous alloying of Pd and Co during the particle growth is not significant in the present nanoparticles 9–16 nm in size because the heat of formation is small (−2 kJ/mol); however, the effect may become prominent for a extremely small nanoparticle[31]. The interfacial alloying and ordering in the present specimen mostly result from thermally activated atom migration because the ordering was not detected for specimens deposited at 573 K (Figure 6). No sign of Co_3Pd was observed in this study, and hence, the existence of an ordered phase in the Co-rich composition is not certain. This result reminds us the similar tendency that no ordered phase exists in Fe-rich Fe–Pd (namely, Fe_3Pd) and Co-rich Co–Pt (Co_3Pt) alloys[10]. It should be mentioned that the Co-Pd alloy forms a solid solution with hcp structure at the Co-rich composition (termed as ε-Co in the phase diagram[9]), in addition to a solid solution with the fcc structure, but this is not an ordered phase.

Ordering Energy and Particle Size Effects on Atom Mixing. We estimated the ordering energy (V_{IJ}) for a binary A–B alloy based on Cowley's theory[25]. V_{IJ} is defined as follows:

$$V_{IJ} = V_{AB,IJ} - \frac{1}{2}\left(V_{AA,IJ} + V_{BB,IJ}\right), \quad (3)$$

where $V_{AB,IJ}$ denotes the interaction energy between an *A* atom with coordinate *I* and a *B* atom with coordinate *J*. If the atom in position *J* is the *k*th nearest neighbor of the atom in position *I*, V_{IJ} is then represented as V_k. Note that $V_{IJ} < 0$ indicates a preference for bonding of A–B atoms rather than A–A or B–B atoms; namely, atomic ordering occurs. The following equation holds between V_{IJ} and the Warren–Cowley parameter (α_i) for the $L1_2$-type ordered structure[25]:

$$k_B T ln\left\{\frac{(1/3+\alpha_i)(3+\alpha_i)}{(1-\alpha_i)^2}\right\} = 2\sum_J V_{IJ}\alpha_i. \quad (4)$$

As a result, we obtained $V_2/|V_1| \approx 0.7$ with $V_1 = -830k_B$ and $V_2 = 569k_B$ assuming the α_i value reported for bulk Co–75at%Pd alloy quenched from 973 K[14]. This result suggests that contribution of the 2nd nearest-neighbor atom is significant in addition to the nearest-neighbor atom with respect to the order–disorder transition in the Co–Pd alloy. The positive value of V_2 indicates that a Co–Co or Pd–Pd pair is preferable for the 2nd nearest-neighbor site (in the fully ordered $L1_2$-type structure, the 2nd nearest neighbor of an atom is the same type atom). This result is in contrast to the case of Cu_3Au alloy, where the nearest-neighbor interaction is dominant ($V_2/|V_1| \approx 0.1$, $V_1 = -358k_B$, $V_2 = 34k_B$ for $T = 678$ K)[25, 32]. It is presumed that the relatively weak interaction of the nearest neighbor (V_1) may result in the absence of LRO in the Co–Pd alloy.

In a small nanoparticle of a few nanometers in diameter (< ~5 nm), either long-range atomic ordering or clustering is restrained and the solid solution may be stabilized[33, 34]. Such a size effect on the structure depends on the Gibbs free energy difference between the ordered phase (or phase separation by clustering) and the solid-solution phase as a function of particle size. The free energy of the SRO embedded in a large-sized particle (> ~10 nm) or a continuous film differs from that of an isolated extremely small nanoparticle, and hence, further study is necessary to elucidate the particle

size dependence of the SRO confined in an interfacial area.

CONCLUSIONS

We studied the local atomic structures of Pd@Co core–shell nanoparticles composed of a Pd core and Co shell using STEM and electron diffraction. Chemically sensitive atomic-resolution Z-contrast imaging revealed the formation of an ordered area 2–3 nm in size within a core–shell nanoparticle. Two types of ordered phases, $L1_2$- and $L1_0$-type, were formed as short- to medium-range order. From electron diffraction studies, we observed an order–disorder transition confined in the interfacial area of core–shell nanoparticles. The transition could only be achieved in the narrow temperature range of 623–723 K, where the diffusion length is limited to a short range comparable to the nearest-neighbor distance. Once the atom migration is activated ($T \geq 773$ K), alloying of Co and Pd proceeds rapidly, and the ordered phase disappears along with the core–shell structure. The combination of HAADF-STEM and electron diffraction is useful for detection of the local atomic configuration in bimetallic nanoparticles. The observation of the ordered phase formation indicates that the magnetic anisotropy of Pd@Co nanoparticles may be enhanced in the future by increasing the volume fraction of ordered phases.

METHODS

Sample Preparation. Sample preparation was performed using a high-vacuum EB deposition chamber with a base pressure of 6×10^{-7} Pa. The Pd@Co nanoparticles were fabricated by sequential deposition of Pd (99.95%), Co (99.98%), and Al_2O_3 (99.99%) onto NaCl(001) single-crystal substrates cleaved in air. The substrate temperature was maintained at 573–673 K during the deposition. A quartz thickness monitor located near the substrate stage in the chamber was used to

control the nominal thickness during the deposition. The deposited thicknesses for Pd, Co, and Al_2O_3 were 0.1–0.9 nm, 0.1–2 nm, and 3 nm, respectively. The average deposition rate of Pd and Co were in the range of 0.05–0.1 nm/min. Note that the nominal thickness differs from the actual nanoparticle thickness (or height) on the substrate surface. By controlling the thickness ratio of Pd and Co, we prepared specimens with an alloy composition ranging between 36 and 89 at%Pd. In this sequential deposition method[26], the Pd nanoparticles act as nucleation sites for the later deposited Co. The size of the Pd seed is approximately 60%–70% of the final nanoparticle size. The finally deposited Al_2O_3 forms a thin amorphous layer, which covers the surface of the Pd@Co nanoparticles.

Characterization. The structure and morphology of the prepared Pd@Co nanoparticles were characterized using a JEOL JEM-ARM200F TEM operating at 200 kV with a CEOS aberration corrector for the probe-forming lens. For STEM imaging, we set the beam convergence to 23 mrad in semi-angle, and HAADF-STEM images were acquired with detector semi-angles of 68–170 mrad. Compositional analyses were performed using an energy-dispersive X-ray spectrometer (EDS; JEOL JED-2300) and a post-column energy filter (Gatan Quantum ER) for electron-energy loss spectroscopy (EELS), both attached to the TEM. The accuracy of the TEM–EDS analysis was estimated to be 1–2% in statistical error of the integrated intensity of the characteristic X-ray. The standard deviation of the alloy composition distribution was 5 at%. *In-situ* TEM observation at elevated temperatures was performed using a specimen heating stage equipped with a Pt–Pt13%Rh thermocouple for temperature measurements. STEM images were simulated using the MACTEMPAS software.

ACKNOWLEDGMENTS

This work was partially supported by a Grant-in-Aid for Scientific Research (JP17H02746) from the

Ministry of Education, Culture, Sports, Science and Technology, Japan. The authors wish to thank Mr. Y. Yamashita and Mr. T. Yasumura for their contribution in this study. The authors would also like to thank Tiffany Jain, M.S., from Edanz Group (www.edanzediting.com/ac) for editing a draft of this manuscript.

AUTHOR INFORMATION

*Email addresses:

sato@uhvem.osaka-u.ac.jp (K. Sato) (corresponding author)

yasuda@uhvem.osaka-u.ac.jp (H. Yasuda)

ORCID

Kazuhisa Sato: 0000-0001-9078-2541

Hidehiro Yasuda: 0000-0002-9877-9803

Author Contributions

All authors contributed to the discussion and writing of the manuscript. The final version of the manuscript was approved by all authors.

Notes

The authors declare no competing financial interest.

REFERENCES

(1) Alloyeau, D.; Mottet, C.; Ricolleau, C. ed. *Nanoalloys. Synthesis, Structure and Properties*; Springer: London, 2012.

(2) Sato, K.; Konno, T. J.; Hirotsu, Y. Electron Microscopy Studies on Magnetic $L1_0$-type FePd Nanoparticles. *Advances in Imaging and Electron Physics*, **2012**, *170*, 165–225.

(3) Andreazza, P.; Pierron-Bohnes, V.; Tournus, F.; Andreazza-Vignolle, C.; Dupuis, V. Structure and Order in CoPt-type Nanoalloys: From Thin Films to Supported Clusters. *Surf. Sci. Rep.* **2015**, *70*, 188–258.

(4) Heemeier, M.; Carlsson, A. F.; Naschitzki, M.; Schmal, M.; Bäumer, M.; Freund, H.-J. Preparation and Characterization of a Model Bimetallic Catalyst: Co-Pd Nanoparticles Supported on Al_2O_3. *Angew. Chem. Int. Ed.* **2002**, *41*, 4073–4076.

(5) Carlsson, A. F.; Bäumer, M.; Risse, T.; Freund, H.-J. Surface Structure of Co-Pd Bimetallic Particles Supported on Al_2O_3 Thin Films Studied using Infrared Reflection Absorption Spectroscopy of CO. *J. Chem. Phys.* **2003**, *119*, 10885–10894.

(6) Napetschnig, E; Schmid, M.; Varga, P. Pd, Co and Co-Pd Clusters on the Ordered Alumina Film on NiAl(110): Contact Angle, Surface Structure and Composition. *Surf. Sci.* **2007**, *601*, 3233–3245.

(7) Shen, K.; Chen, L.; Long, J.; Zhong, W.; Li, Y. MOFs-Templated Co@Pd Core-Shell NPs Embedded in N-Doped Carbon Matrix with Superior Hydrogenation Activities. *ACS Catal.* **2015**, *5*, 5264–5271.

(8) Kovács, A.; Sato, K.; Hirotsu, Y. Structure and Magnetic Properties of Nanocrystalline Pd-Co and Pd-Co-Fe Layers. *Solid State Phenomena* **2007**, *124–126*, 907–910.

(9) Ishida, K.; Nishizawa, T. The Co-Pd (Cobalt-Palladium) System. *J. Phase Equilibria* **1991**, *12*,

83–87.

(10) Massalski, T. B.; Okamoto, H.; Subramanian, P. R.; Kacprzak, L. ed. *Binary Alloy Phase Diagrams*, 2nd ed.; ASM International: Ohio, 1990.

(11) Kumar, S.; Iizuka, Y,; Xu, Q. Nickel-Palladium Nanoparticle Catalyzed Hydrogen Generation from Hydrous Hydrazine for Chemical Hydrogen Storage. *International J. Hydrogen Energy* **2011**, *36*, 11794–11801.

(12) Zhang, M.; Yan, Z.; Sun, Q.; Xie, J.; Jing, J. Synthetic Core-Shell Ni@Pd Nanoparticles Supported on Graphene and Used as an Advanced Nanoelectrocatalyst for Methanol Oxidation. *New J. Chem.* **2012**, *36*, 2533–2540.

(13) Rai, R. K.; Gupta, K.; Behrens, S.; Li, J.; Xu, Q.; Singh, S. K. Highly Active Bimetallic Nickel-Palladium Alloy Nanoparticle Catalyzed Suzuki-Miyaura Reactions. ChemCatChem **2015**, *7*, 1806–1812.

(14) Katsnel'son, A. A.; Alimov, Sh. A.; Dazhayev, P. Sh.; Silonov, V. M.; Stupina, N. N. Local Ordering and the Resistivity of Ni-W and Pd-Co Alloys. *Phys. Met. Metallogr.* **1968**, *26*, 26–35.

(15) Matsuo, T. Ordered Alloys in the Cobalt-Palladium System. *J. Phys. Soc. Jpn.* **1972**, *32*, 972–978.

(16) Ostanin, S.; Razee, S. S. A.; Staunton, J. B.; Ginatempo, B.; Bruno, E. Magnetic Anisotropy and Compositional Order in $Fe_{0.5}Pt_{0.5}$: Calculations from an *Ab-initio* Electronic Model. *J. Appl. Phys.* **2003**, *93*, 453–457.

(17) Hirotsu, Y.; Ohkubo, T.; Matsushita, M. Study of Amorphous Alloy Structures with Medium Range Atomic Ordering. *Microsc. Res. Tech.* **1998**, *40*, 284–312.

(18) Hata, S.; Matsumura, S.; Kuwano, N.; Oki, K. Short Range Order and Its Transformation to Long Range Order in Ni_4Mo. *Acta Mater.* **1998**, *46*, 881–892.

(19) Niu, C.; Zaddach, A. J.; Oni, A. A.; Sang, X.; Hurt III, J. W.; LeBeau, J. M.; Koch, C. C.; Irving, D. L. Spin-Driven Ordering of Cr in the Equiatomic High Entropy Alloy NiFeCrCo. *Appl. Phys. Lett.* **2015**, *106*, 161906.

(20) Sato, K.; Wen, J. G.; Zuo, J. M. Intermetallic Ordering and Structure in Fe-Pd Alloy Nanoparticles. *J. Appl. Phys.* **2009**, *105*, 093509.

(21) Sato, K.; Yanajima, K.; Konno, T. J. Structure and Compositional Evolution in Epitaxial Co/Pt Core-Shell Nanoparticles on Annealing. *Thin Solid Films* **2012**, *520*, 3544–3552.

(22) Sato, K.; Matsushima, Y.; Konno, T. J. Surface-Segregation-Induced Phase Separation in Epitaxial Au/Co Nanoparticles: Formation and Stability of Core-Shell Structures. *AIP Adv.* **2017**, *7*, 065309.

(23) Warren, B. E. *X-ray Diffraction*; Dover Publications, Inc.: New York, 1990.

(24) Bethe, H. A. Statistical Theory of Superlattices. *Proc. Roy. Soc.* **1935**, *150A*, 552–575.

(25) Cowley, J. M. An Approximate Theory of Order in Alloys. *Phys. Rev.* **1950**, *77*, 669–675.

(26) Bian, B.; Sato, K.; Hirotsu, Y.; Makino, A. Ordering of Island-like FePt Crystallites with Orientations. *Appl. Phys. Lett.* **1999**, *76*, 3686–3688.

(27) Vitos, L.; Ruban, A. V.; Skriver, H. L.; Kollár, J. The Surface Energy of Metals. *Surf. Sci.* **1998**, 411, 186–202.

(28) Swalin, R. A. *Thermodynamics of Solids*; John Wiley & Sons, Inc.: New York, 1962.

(29) de Boer, F. R.; Boom, R.; Mattens, W. C. M.; Miedema, A. R.; Niessen, A. K. *Cohesion in Metals: Transition Metal Alloys (Cohesion and Structure)*; North-Holland: Amsterdam, 1988.

(30) Iijima, Y.; Hirano, K. Interdiffusion in Co-Pd Alloys. *Trans. JIM* **1972**, *13*, 419–424.

(31) Yasuda, H.; Mori, H.; Furuya, K. Spontaneous Atom Mixing and Unmixing in Metallic Nanoparticles. *Phil. Mag. Lett.* **2000**, *80*, 181–186.

(32) Cowley, J. M. X-ray Measurement of Order in Single Crystals of Cu_3Au. *J. Appl. Phys.* **1950**, *21*, 24–30.

(33) Yasuda, H.; Mori, H. Effect of Cluster Size on the Chemical Ordering in Nanometer-Sized Au-75at%Cu Alloy Clusters. *Z. Phys. D* **1996**, *37*, 181–186.

(34) Christensen, A.; Stoltze, P.; Nørskov, J. K. Size Dependence of Phase Separation in Small Bimetallic Clusters. *J. Phys. Condens. Matter.* **1995**, 7, 1047–1057.